ISSN 0016-7029, Geochemistry International, 2017, Vol. 55, No. 3, pp. 263–281. © Pleiades Publishing, Ltd., 2017.

Geochemistry and Nd, Sr Isotopes of the Pohrenk Fluorites (Kırsehir-Turkey)[1]

Y. Uras[a], *, A. V. Nikiforov[b], F. Oner[c], and O. Parlak[d]

[a]*Kahramanmaras Sutcu Imam Universty, Department of Geological Engineering, Avsar Campus, Kahramanmaras, Turkey*
[b]*Insitute of Geology of Ore Deposits, Petrography Mineralogy and Geochemistry, Russian Academy of Sciences, Moscow, 119017 Russia*
[c]*Mersin Universty, Department of Geological Engineering, Ciftlik Campus, Mersin, Turkey*
[d]*Cukurova Universty, Department of Geological Engineering, Balcali Campus, Adana, Turkey*
**e-mail: yuras@ksu.edu.tr*

Received July 15, 2015; in final form, January 26, 2016

Abstract—The Pohrenk fluorite mineralisation which makes up Central Anatolia's most extensive fluorite region is Lutetian aged, and hosted in carbonate rocks that have undergone occasional karstification and silicification along a N–S fault trend. Fluid inclusion values and the position of fluorites in the Tb/La–Tb/Ca diagram show that mineralisation occurred in a hydrothermal environment with homogenisation temperatures ranging from 78.1–363°C. The presence of fluorite as a space filler in carbonate rocks and its association with silicification indicates that the solutions contained considerable amounts of Si alongside F (fluorine). The Pohrenk fluorite samples have $^{143}Nd/^{144}Nd$ values of between 0.512349 and 0.512497, whilst $^{87}Sr/^{86}Sr$ values vary between 0.708161 and 0.708772. These values indicate a mantle origin where continental contamination could occur. When the Nd–Sr values are compared to magmatic and young volcanics, the Pohrenk fluorites are seen to be enriched and exhibit similar isotopic signatures to Upper Cretaceous aged magmatics, Early-Middle Miocene volcanics and Mio-Quaternary volcanics.

Keywords: Pohrenk (Kırsehir), Fluorite, Rare Earth Elements, Fluid Inclusions, Isotope

DOI: 10.1134/S0016702917030090

1. INTRODUCTION

Fluorite, which is present in many mineral deposits as either a gangue or ore mineral, generally occurs as a primary mineral in lead-zinc deposits (Constantopoulos, 1988; Eppinger, 1988). The study area encompasses the fluorite beds near Pohrenk village, north of Kırşehir (Fig. 1). The aim of this study was to define the conditions and processes that facillitated the fluorite mineralisation seen in the sedimentary rocks in and around Pohrenk village. To accomplish this aim, petrographic, mineralogical, geochemical properties and isotope analyses were carried out on the Pohrenk fluorite mineralisation. The majority of karstic spaces are filled with limestone blocks and clay material in the Pohrenk fluorite area. The filler surrounding the limestone is well crystallised, honey-coloured and contains considerable amounts of fluorite, barite, calcite and sulphur. Fluoridised nummulites and lamellibranch shells can be found alongside the Pohrenk fluorites.

2. SAMPLING AND ANALYTICAL METHODS

In addition to the systematic sampling performed within the valley, sampling of the Pohrenk fluorite for XRD, FTIR, petrographic and geochemical analysis was carried out on the clay unit overlying the fluorite formation, the formation unit in the Dulkadir limestone wallrock, the nummulite shells in the limestone and waste from the fluorite (Table 1). Samples were also taken from the travertines formed around the hot water sources (Table 1). The quantitative XRD and fluid inclusion analyses were completed at M.T.A (General Directorate of Mineral Research and Exploration). The fluid inclusions in the fluorite samples were studied from a morphological, thermometric and cryoscopic point of view to define the temperature and chemical conditions present during the mineralisation of the Pohrenk fluorite. Fluid inclusion studies were conducted on primary and secondary inclusions using thermo-optic measurements. The separation of both inclusion groups from one another was completed according to geometric crystals. The mineralogical composition of all samples was determined in the C.U faculty of science and letters Chemistry Department using the KBr-tablet technique of the FTIR (Fourier Transform Infrared Spectroscopy) method. The prepared 10 gram samples were analysed by ICP-ES in the ACME (Canada) Laboratory to gauge major-oxide, fluoride and trace element contents. Further-

[1] The article is published in the original.

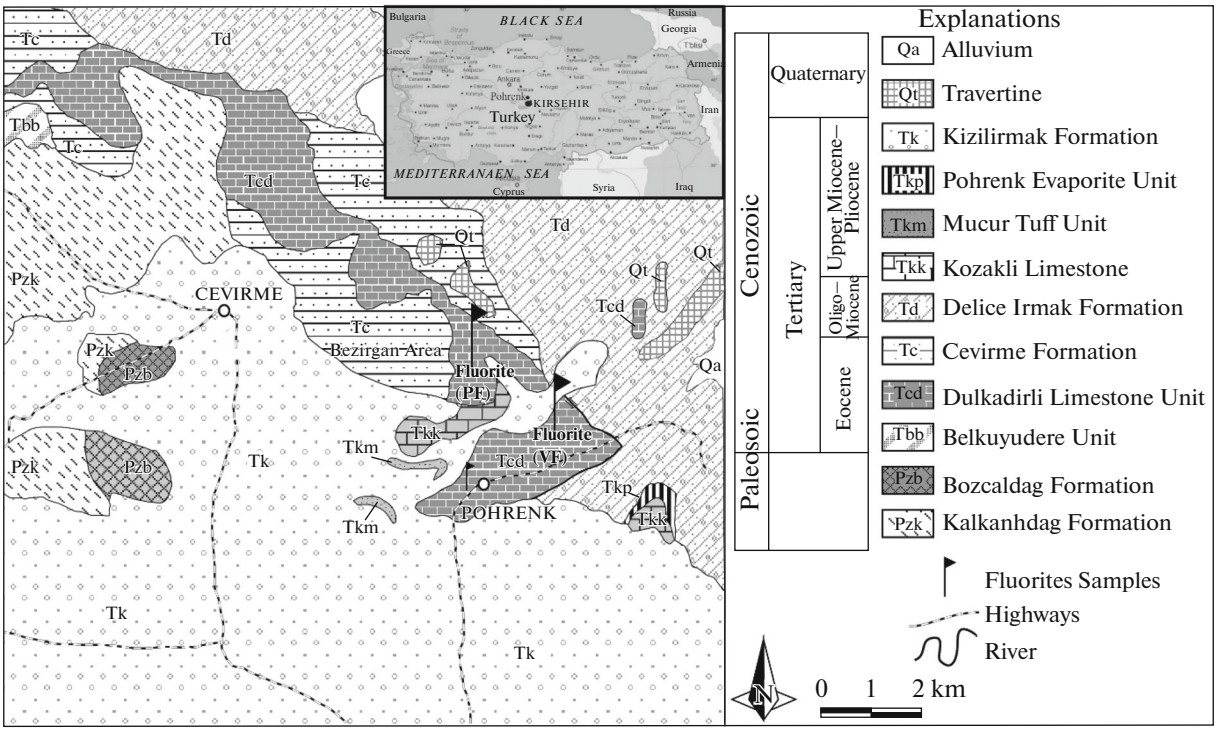


Fig. 1. General geology and location map of Pohrenk (Kirsehir) Bezirgan area (M.T.A., 1991).

more, rare earth element contents were determined using ICP-MS. ICP-MS measures the element concentrations by counting the atoms for each element present in the solution. Typically the ICP-MS packages are selected for soil, till and sediment surveys to provide the broadest array of elements coupled with lowest detection limits to ensure maximum exploration power.

The Sm–Nd and Rb–Sr studies were carried out by A.V. Nikiforov at the Laboratory of Isotope Geology and Geochronology of the Institute of Geology of Ore Deposits, Petrography, Mineralogy, and Geochemistry, Russian Academy of Sciences (RAS), using the standard technique and the isotope dilution method (Chernyshev et al., 1983; Zhuravlev et al., 1983). The isotope ratios of Rb, Sr, Sm and Nd were measured on a Sector-54 mass spectrometer in the static ore multidynamic regime. The concentrations of the elements were determined with an accuracy of 1% rel. Isotopic ratios were measured with an accuracy of (2σ) 0.5% rel. for $^{87}Rb/^{86}Sr$ and 0.15% rel. for $^{147}Sm/^{144}Nd$. Parallel analyses yielded the following results for standard samples: $^{143}Nd/^{144}Nd = 0.511840 \pm 12$ for La Jolla ($2\sigma_{un}N = 19$, normalized to $^{146}Nd/^{144}Nd = 0.7219$) and $^{87}Sr/^{86}Sr = 0.710245 \pm 19$ for SRM-987 ($2\sigma_{un}N = 16$, normalized to $^{84}Sr/^{88}Sr = 0.1194$). The blank levels during measurements were 0.05 ng for Rb, 0.2 ng for Sr, 0.1 ng for Sm and 0.2 ng for Nd. It was

Table 1. Samples taken from the formations of the Dulkadir limestone unit in the Bezirgan Area

Sampling		Number	Sample number
Formations in the Dulkadir limestone unit		11	A-2, A-4, A-5, A-6, A-7, A-8, A-9, A-10, A-11, A-14, A-15
Clay		3	KC-5,KJ-1,KO-1
Travertine		14	TB-1, TB-2, TB-3, TB-4, TB-5, TB-6, TB-8, TB-9, TB-10, TB-11, TB-12, TB-13, TBH-1
Nummulite		3	NT-1, NK-1, NK-2
Barite		1	BT-1
Fluorite	Valley	8	VF-1, VF-2, VF-3, VF-4, VF-5, VF-6, VF-7, VF-8
	Waste	10	PF-1, PF-2, PF-3, PF-4, PF-5, PF-6, PF-7, PF-8, PF-9, PF-10

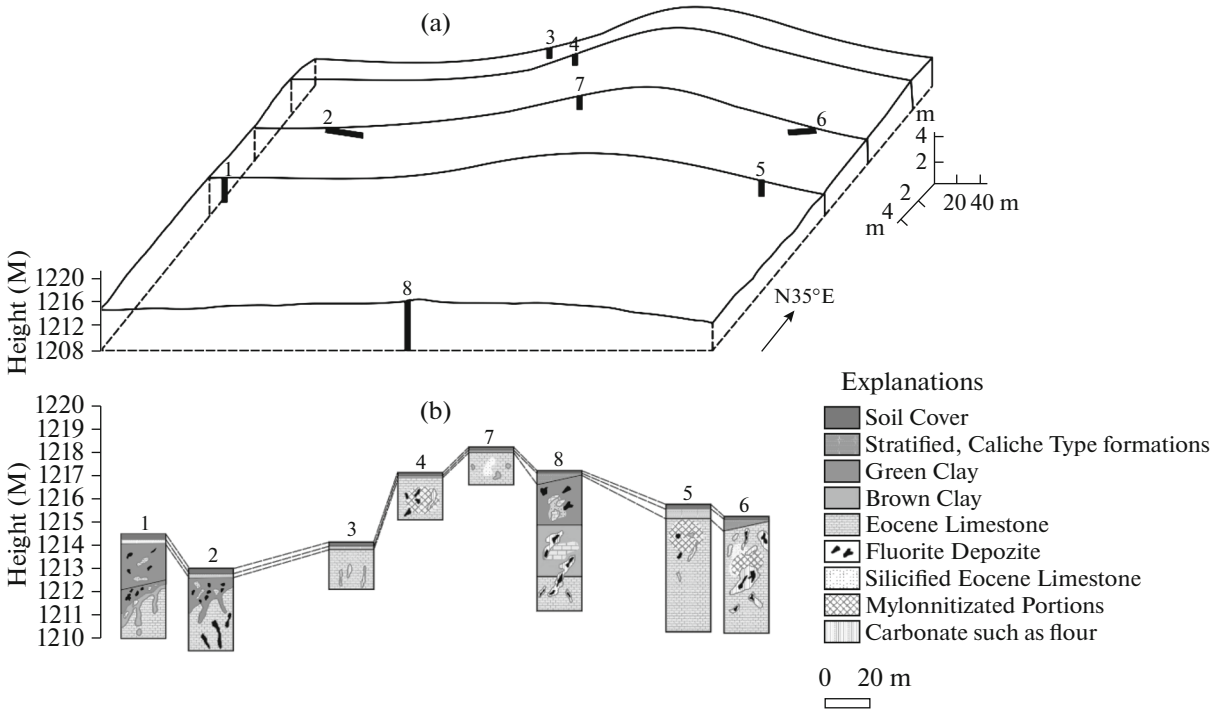


Fig. 2. (Waste) well and gallery sections of the Bezirgan area (edited from M.T.A., 1991).

not possible to calculate the age of the fluorite due to the very small Rb/Sr ratio.

3. GEOLOGY OF THE STUDY AREA

Palaeozoic and Cenozoic aged units are found in and around the study area. In order from oldest to youngest these units are: Palaeozoic aged Kalkandag and Bozcaldag Formations, Dulkadir limestone units and Belkuyudere member of the Eocene aged Cevirme Formation, Oligocene-Miocene aged Delice Irmak Formation, Upper Miocene and Pliocene aged Kozakli limestone, Mucur tuff units, Pohrenk evaporite units and the Kizilirmak Formation and Quaternary aged travertine and alluvium units at the surface (Fig. 1). The fluorite formation subject to this study is part of the Cevirme Formation, representing a transgressive series with parallel laminated and well-formed sandstone-siltstone at the lower levels, interbedded with white, beige-cream coloured, medium-thick layered massive limestone at higher levels, containing mudstone with mussel fragments (Oktay, 1981 and M.T.A., 1991). The Dulkadir limestone member (Tcd) of the Cevirme Formation is situated in the northern segment of the study area. The Dulkadir limestone member is found with limestone at the top and edges of the Cevirme Formation with abundant nummulites, coral, gastropods and features laminated, white, beige-cream coloured, medium-thick layered, occasionally massive, with carbonate mud case-stack-grain boundstone properties (Oktay, 1981). The size of fluorite in the Bezirgan area of this unit is small. The fluorite found in the valley southeast of the Bezirgan area is larger in size. When the well and gallery sections of the Bezirgan area are studied this sequence is seen: soil cover at the top, layered caliche type formations, green clay, brown clay, Eocene aged limestone, fluorite mineralisation, silicified Eocene aged limestone, mylonitised sections, floury carbonate at the base (Figs. 2, 3). Fluorine values of 5 ppm were determined by (Uras and Calıskan, 2011) from the hot and cold waters that formed the white, beige, cream, light brown, light green coloured travertine (Qt) which outcrops in Mahmutlu and developed from the recent tectonic movements affecting the region.

4. MINERALOGY

In petrographic analyses of the Dulkadir limestone, alongside the fluorite, clay alteration forming a laminated texture with shell fragments was defined (Figs. 4a, 4b). Fluorite and quartz mineralisation is seen in thin sections (Fig. 4c). Fluorite mineralisation is seen as thin vein systems with an epigenetic character or as space filling. Chalcedony-like quartz is widespread both in the wall rock and within the mineralisation. The quartz minerals are of different sizes, anhedral and in places as crystals with sharp corners. The quartz which is seen in different proportions through the rock shows a good distribution overall. The wavy extinction shown by the quartz crystals indicates that they underwent deformation as a result of hot water or pressure



Fig. 3. The formations of the Dulkadir limestone unit in the Bezirgan area.

(Fig. 4d). The fluorite crystallised by encompassing quartz and silicified marl fragments, highlighting the carbonate layers. The substitution of $CaCO_3$ shells belonging to nummulites and echinoderms in the limestone by fluorite was determined through macro and micro observations (Figs. 4e, 4f).

The FTIR diagrams of the formations in the Dulkadir limestone member around the fluorite of the Pohrenk area are given in A-2 (Fig. 5a), A-7 (Fig. 5b), A-14 (Fig. 5c), KO-1 (Fig. 5d), TB-8 (Fig. 5e) and BT-1 (Fig. 5f). These samples were selected as they show the same minerals as the other samples. In Fig. 5b, the presence of kaolinite was determined from peaks at 3698, 3664 and 3621 cm^{-1} caused by OH, whilst the double peak at 798 and 778 cm^{-1} indicates quartz. In some samples, there are peaks belonging to dickite at 3700, 3710 cm^{-1} (Fig. 5a). Other than kaolin and dickite, smectite and illite are also seen in some samples (Figs. 5c, 5d, 5e). These minerals typically show peaks between 3620 and 3630 cm^{-1}. Samples containing carbonate are characterised by the so called carbonate peak at 1400 cm^{-1} (Fig. 5b). FTIR analyses revealed that the carbonate component of the samples is calcite (712 cm^{-1}). Apatite is observed in one sample, characterised by peaks at 1432 and 1452 cm^{-1} (Fig. 5e). Furthermore, barite is seen with fluorite in the mineralisation zone (Fig. 5f). KO-1 is kaolinite, illite-smectite and quartz. KC-5 is kaolinite (dickite), smectite and quartz. NT-1 (nummulite sample) is pure calcite. NK-1 and NK-2 samples are taken from the rock alongside the nummulite, and the samples contain kaolinite, quartz and calcite. The samples taken from the formations of the Dulkadir limestone member were also analysed by XRD (Fig. 6). From these samples, KC-5 was selected because the same minerals were seen in all samples. The main components are quartz and kaolinite. In some samples calcite, feldspar and illite-smectite group clay are also present. There are important peaks at 12, 34–62, 36–24, 88 in the kaolinite XRD diagram. In the quartz XRD diagram, whilst quartz is shown by peaks at 26, 21–20, 46 and 49, 63, calcite is seen at peaks at 29, 43–39, 43 and 43, 18. In some samples there are peaks belonging to illite and smectite group minerals at 10 and 16°A. The results of the XRD analyses match the FTIR results.

5. FLUID INCLUSION DATA

In the honey-yellow coloured fluorite samples PF-1 and VF-1 completely made up of transparent fluorite crystals there is a medium abundance of primary fluid inclusions and a large abundance of secondary fluid inclusions developed along micro fractures within the mineral (Figs. 11a, 11b). The large majority of primary fluid inclusions used for the measurements contained both liquid and gas phases. The study of the histograms acquired from the 13 microthermometric (PF-1) measurements and 18 microthermometric (VF-1) results show that the PF-1 fluorite crystal had a homogenisation temperature of 102–363°C, whilst VF-1 varied between 70–210°C (Table 2). PF-1 increases at 220–250°C whilst VF-1 increases in abundance at 100–110°C (Figs. 7, 8).

The presence of both single phase liquid and single phase gas inclusions in the same environment allowed homogenisation temperatures to be taken directly as formation temperatures. The primary rooted 2-phased (liquid+gas) inclusions from which homogenisation temperatures (Th°C) were measured in the fluorite crystal fragments, were frozen using liquid nitrogen and ice melting temperatures (Tice-m°C) were calculated. The PF-1: 24 and VF-1: 14 measured ice melting temperatures (Tice-m°C) and their corresponding %NaCl equivalent are given in Table 3. The %NaCl

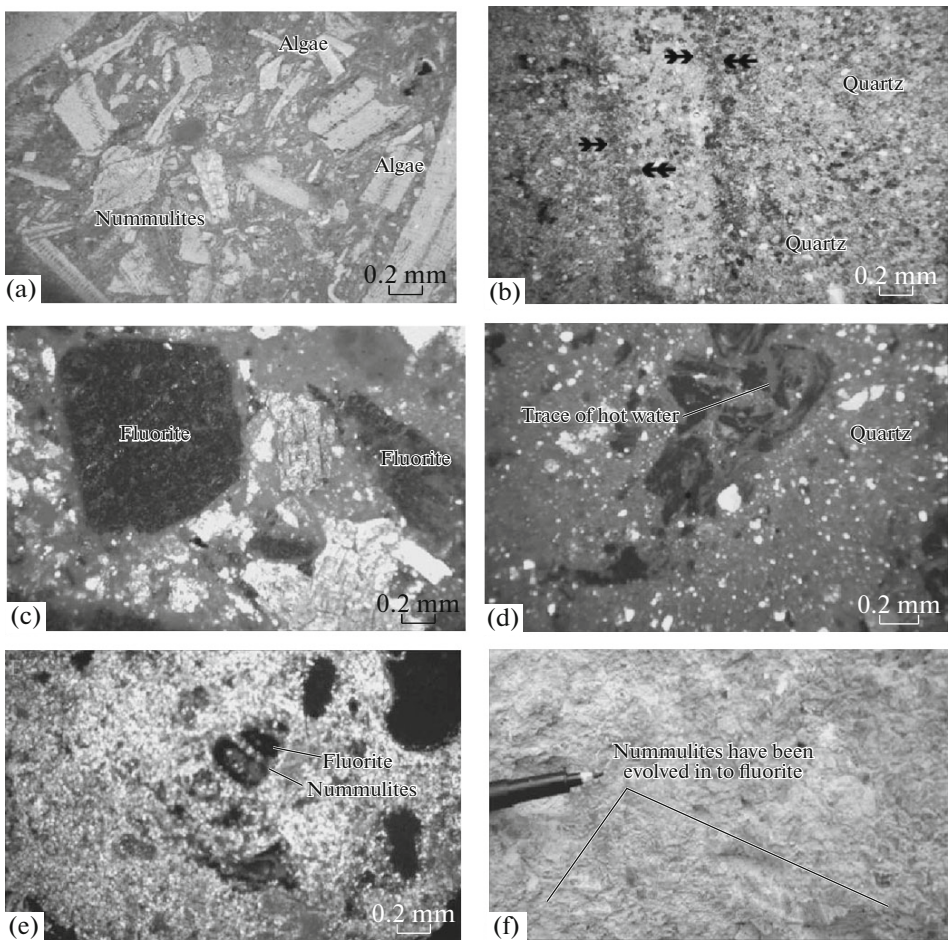


Fig. 4. (a) Fossil shells from the wall rock; (b) laminated clay alteration; (c) fluorite formation; (d) quartz mineralisation and hot water traces; (e) fluoridised nummulite shells in thin section; (f) macro appearance of fluoridised nummulite shells.

value of the solution was calculated according to (Bodnar, 1993). According to Table 3, the 24 salinity values calculated from ice melting temperatures measured from PF-1 fluorite crystal were 1.05–24.08% whilst the 14 salinity values for VF-1 varied between 0–22.78%. Increase in salinity between 22–24% PF-1, 0–3% VF-1 of the solution that formed PF-1 and VF-1 fluorite crystals indicates that there was a progressive decrease in solution salinity from 20% to 1% NaCl for PF-1 and 22.78% to 0% NaCl for VF-1 (Figs. 9, 10). From a morphological point of view, the primary inclusions in both PF-1 and VF-1 (Figs. 11a, 11c) of 30–40 μ and larger show a distribution perpendicular to crystallisation surfaces. All of the primary inclusions contain two phases comprising liquid and gas. These two phased inclusions show a homogenous distribution in all samples studied. This observation highlights the formation of fluorite in stable physicochemical conditions. Secondary inclusions are situated in cleavages or along crystal fracture sutures. These inclusions attract attention with their elongated shape, varying sizes and occasional variation in content. The

Table 2. Homogenisation temperatures of the Pohrenk fluorites (PF-1 and VF-1)

Homogenisation Temperatures (Th°C)	PF-1										
	102	103	107	235	246	249	250	265	282	309	353
	355	363									
	VF-1										
	78.1	86.8	90.7	100	102.4	107.7	107.8	108	110	114.6	118
	124	142.3	144.5	174.2	176.1	203.7	210.9				

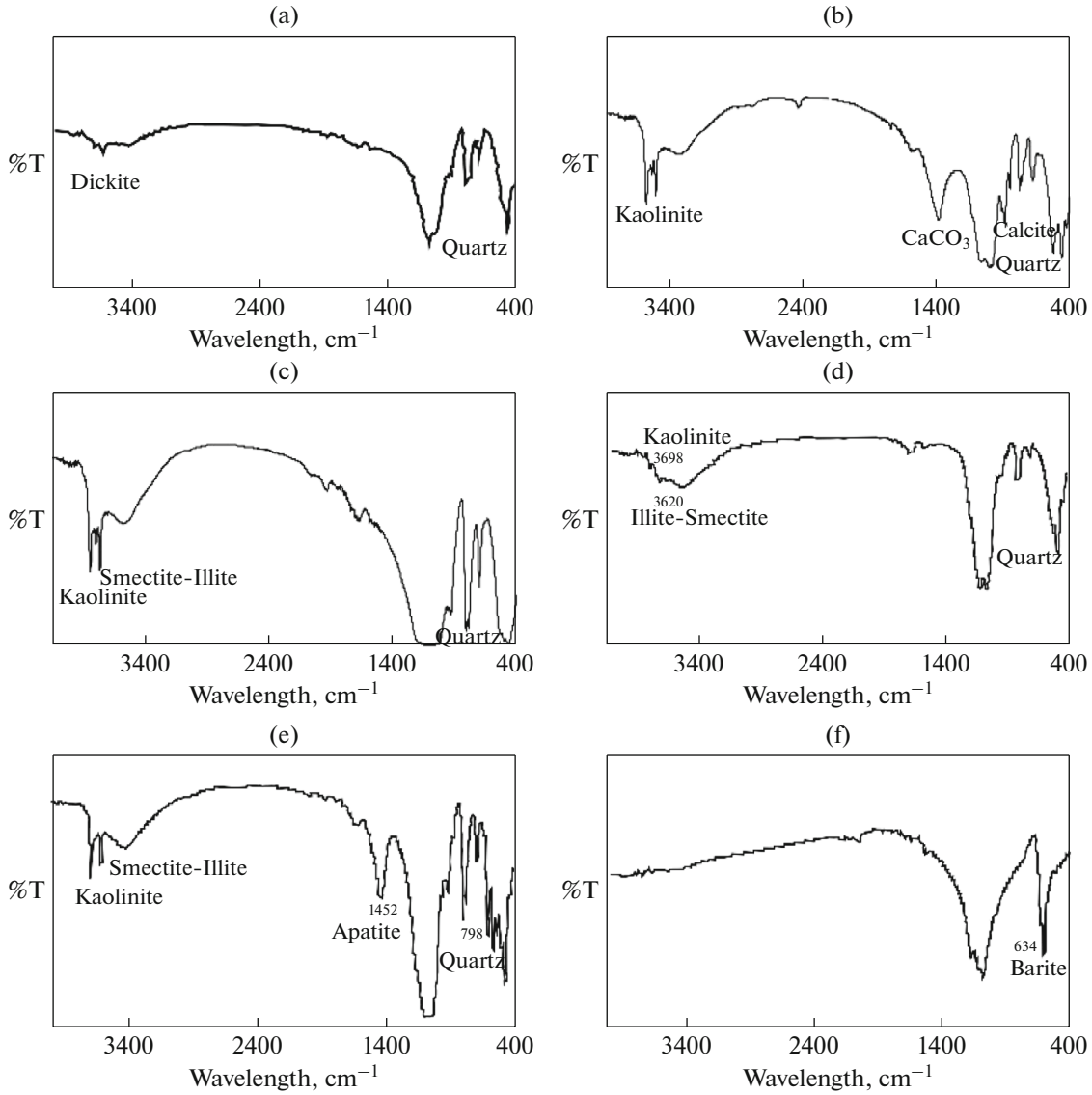


Fig. 5. (a) FTIR diagram of dickite and quartz; (b) FTIR diagram of kaolinite, quartz and calcite; (c) FTIR diagram of smectite-illite, kaolinite and quartz; (d) FTIR diagram of illite-smectite; (e) FTIR diagram of apatite; (f) FTIR diagram of barite.

abundant secondary inclusions (Figs. 11b, 11d) indicate that the secondary environment conditions continued to affect previous crystallisations at the end of the crystallisation period. The presence of barite in the paragenesis suggests that the mineralisation environment began to cool after the major fluorite crystallisation stage. According to experimental results, barite concentration values reach a maximum at approxi-

Table 3. Tice-m (°C) and %NaCl values of the Pohrenk fluorites (PF-1 and VF-1)

PF-1	Tice-(°C)	% NaCl	Tice-(°C)	% NaCl	Tice-(°C)	% NaCl	Tice-(°C)	% NaCl	Tice-(°C)	% NaCl
	−0.6	1.05	−4.5	7.17	−20.5	22.71	−20.8	22.91	−6.5	9.86
	−2.5	4.18	−4.9	7.73	−20.8	22.91	−20.9	22.98	−11.0	14.97
	−2.7	4.49	−20.2	22.51	−20.8	22.91	−21.0	23.05	−11.3	15.27
	−18.0	20.97	−20.0	22.38	−21.3	23.24	−21.4	23.31	−21.6	23.44
	−21.8	23.57	−22.0	23.72	−22.6	24.08				
VF-1	Tice−(°C)	% NaCl	Tice−(°C)	% NaCl	Tice−(°C)	% NaCl	Tice−(°C)	% NaCl	Tice−(°C)	% NaCl
	0	0	−0.3	0.53	−0.9	1.57	−19.8	22.24	−20.5	22.71
	0	0	−0.4	0.70	−2.0	3.39	−20.1	22.44	−20.6	22.78
	0	0	−0.8	1.40	−2.5	4.18	−20.4	22.65		

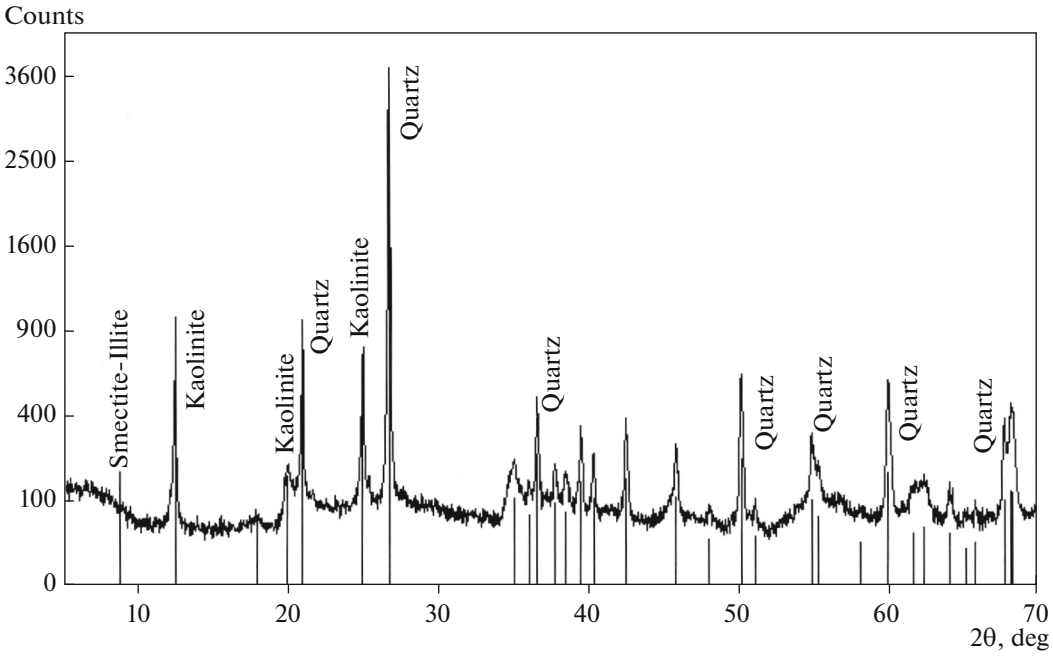


Fig. 6. The appearance of KC-5 from the Dulkadir limestone member on an XRD diagram.

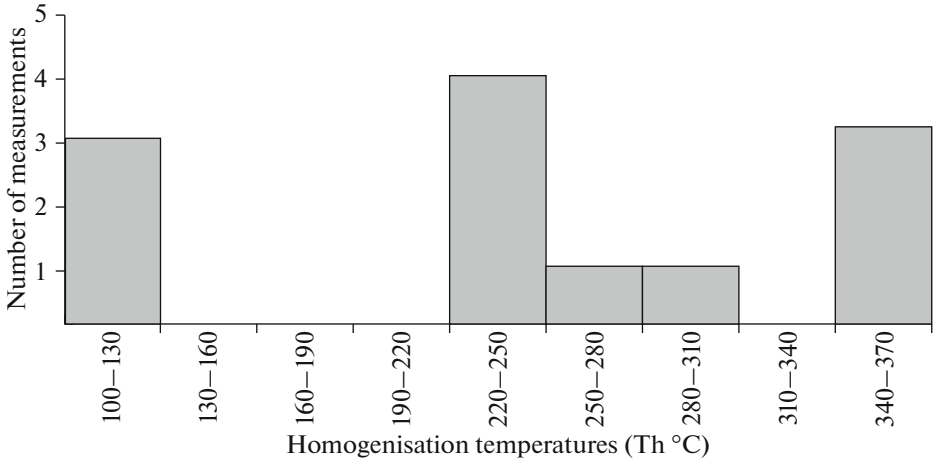


Fig. 7. Diagram showing the homogenisation temperature of PF-1.

mately 75°C. The variable salinity values shown by the secondary inclusions reveal that first of all, there could be different salt quantities in the environment. This could be explained by the continued dilution of mineralising fluids during mineralisation which is possible with the likely mixing of meteoric water with deep rooted saline meteoric waters. The homogenisation (Th) temperature of the inclusions could vary according to the primary pressure. It is, however, possible that the mineralisation environment developed at shallow depth. The coral limestone, which makes up the wall rocks, the terrestrial Pliocene units and the continuous presence of calcite during paragenesis shows that the mineralisation is not at a deep enough level to require a pressure correction in the Th value. Therefore, it can be argued that following forming the first fluorite crystals at high temperatures (between 220–370°C) the salinity levels of the solution became increasingly low and diluted and likely mixed with meteoric waters. To conclude, the PF-1 and VF-1 fluorite crystals probably started to form in a hydrothermal-mesothermal phase and continued forming in the epithermal phase. Furthermore, in the study by (Uras and Calıskan, 2011) on the root of the hot and cold waters at Pohrenk and the surroundings, it was shown that the waters were meteorically rooted.

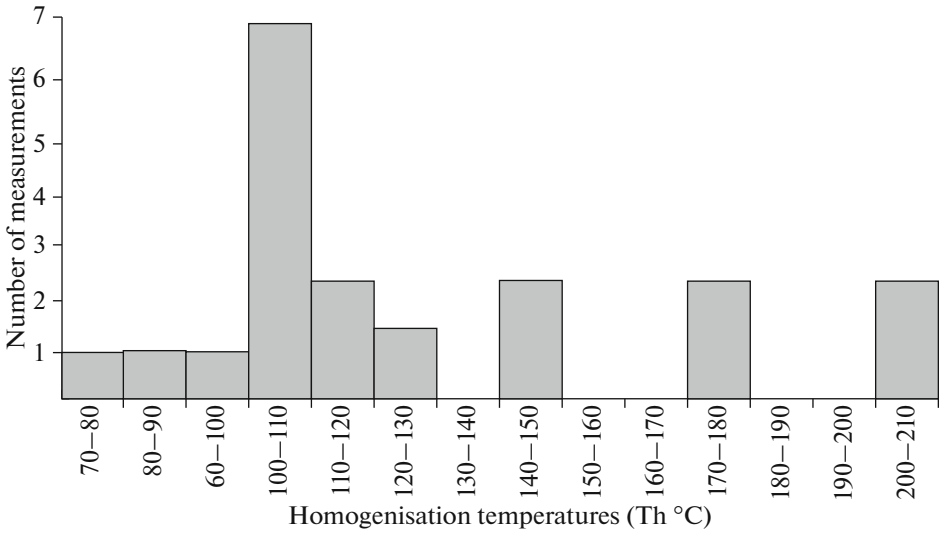


Fig. 8. Diagram showing the homogenisation temperature of VF-1.

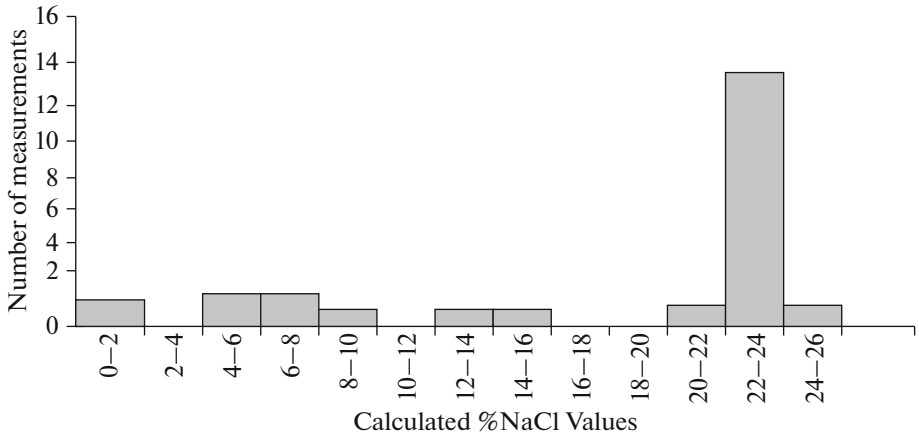


Fig. 9. Diagram showing calculated %NaCl values of PF-1.

6. THE REE GEOCHEMISTRY

The major and trace element content of the Pohrenk fluorite samples from the analyses are given in Tables 4 and 5. Apart from two samples (VF-1 and VF-9), the major element content of all the fluorite samples are found to be made of pure fluorite. Sample VF-9 is made of silica and fluorite and the silica phase (Opal $SiO_2 \cdot nH_2O$) contains a considerable amount of water (LOI 4.2%). All major oxide contents of the samples are less than 0.5%, apart from CaO. The trace element content of the fluorite samples indicate the occurrence of important changes. For example, whilst Ba concentration ranges from 4.5 ppm to 1752 ppm, Sr ranges between 31–71 ppm and Y ranges between 6.5–28 ppm. The Rb, Zr, Nb, Hf, Ga, Cs, U and Th (apart from VF-2) values of the fluorites are very low and below 1 ppm.

The major element analysis results of the formations and of the clay, barite, nummulite and travertine of the Dulkadir limestone member surrounding the fluorite belonging to the Pohrenk region are given in Table 6. The SiO_2 content of the formations vary between 86.0–16.0%, 4.23–22.02% Al_2O_3, 0.62–5.44% Fe_2O_3, 0.26–1.94% MgO, 0.4–41.9% CaO, 0.01–0.42% Na_2O and 0.48–2.91% K_2O whilst TiO_2, P_2O_5, MnO and Cr_2O_3 content is less than 1%. The chemical composition of BT-1 found alongside the fluorite shows that this sample is made of pure barite. The sample KJ-1 taken from the thin white layer above the fluorite mineralisation is made of $CaCO_3$. The nummulites and limestone containing these fossils have an element content varying between: 1.29–67.51% SiO_2, 0.41–15.82% Al_2O_3, 0.12–2.47% Fe_2O_3, 1.8–55.9% CaO and 0.04–2.91% K_2O. From the

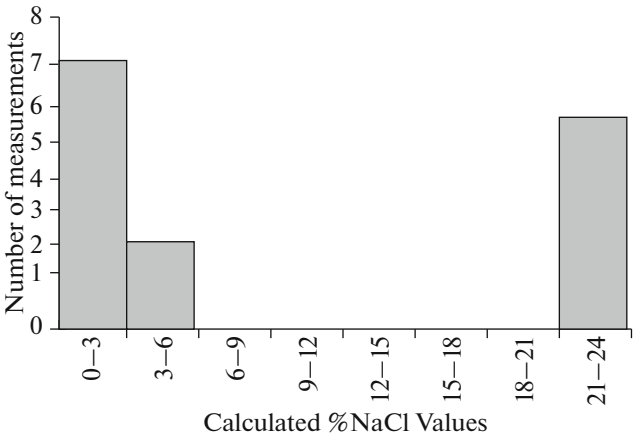


Fig. 10. Diagram showing calculated %NaCl values of VF-1.

other oxides, MgO, Na_2O, TiO_2, P_2O_5, MnO and Cr_2O_3 have low concentration and are less than 0.5%. The chemical composition of travertines varies between 87.75–57.39% SiO_2, 6.53–10.68% Al_2O_3, 0.38–2.46% Fe_2O_3, 0.27–0.46% MgO, 0.1–15.4% CaO, 0.02–0.11% Na_2O, 0.59–1.13% K_2O, 0.34–0.52% TiO_2, and 0.04–9.24% P_2O_5. MnO and Cr_2O_3 are 0.01%. Furthermore, one travertine sample (TBH-1) contained only CaO and CO_2 and was made of pure calcite. The trace element analysis results of the formations, clay, travertine and nummulite (NT-1, NK-1 and NK-2) of the Dulkadir limestone member surrounding the Pohrenk fluorite are given in Table 7. When average trace element values of clay units are studied, Ba shows important changes (Ba 64–8870 ppm). Sample A2 which has a high Ba concentration also contains 0.22% S which demonstrates that this sample contains the barite mineral ($BaSO_4$). Other trace element values range between 79–238 ppm Sr, 18–98 ppm Rb, 0.8–0.4 ppm Hf, 2.3–10.5 ppm Nb, 4.5–2.4 ppm Ga, 4.0–18.3 ppm Cs, 1.5–10.7 ppm Th, 28–146 ppm Zr and 4–18.7 ppm Y. Trace element content of the nummulites varies between 106–174.1 ppm Sr, 1.20–81.70 ppm Rb, 0.5–3.30 ppm Hf, 0.5–11.70 ppm Nb, 0.60–28.10 ppm Ga, 0.40–32.60 ppm Cs, 2.70–15.40 ppm Th and 3.40–109.80 ppm Zr (Table 7). Trace element content of the travertines varies between 764.4–76.1 ppm Sr, 53.90–3.30 ppm Rb, 0.5–2.20 ppm Hf, 0.5–8.30 ppm Nb, 1.60–15.40 ppm Ga, 1.40–22.70 ppm Cs, 0.20–7.70 ppm Th and 119.20–4.00 ppm Zr (Table 7). In the travertine and wall rock outside the fluorite and nummulite there is a good relationship between HFS (High Field Strength) elements Zr, Hf, Nb and Ga (r = >0.8). These elements are known to make up the same type of mineral.

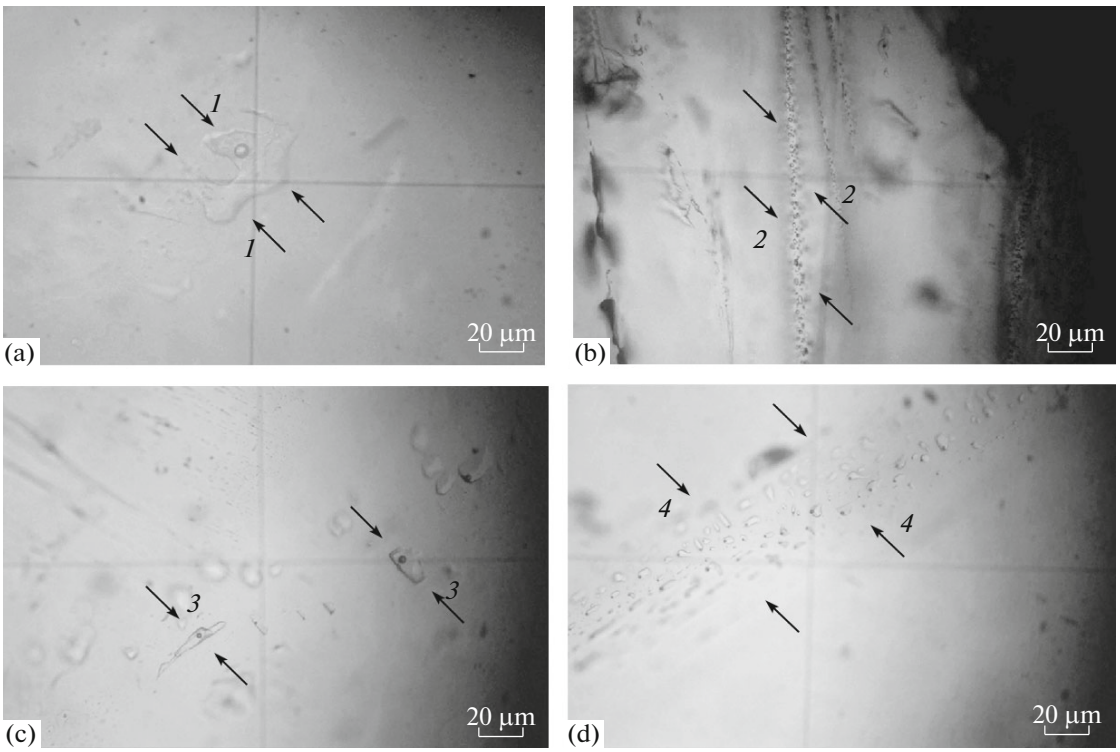


Fig. 11. (a) Microscopic view of a primary rooted fluid inclusion of the PF-1 fluorite sample in the fluid inclusion study; (b) microscopic view of a secondary rooted fluid inclusion of the PF-1 fluorite sample in the fluid inclusion study; (c) microscopic view of a primary rooted fluid inclusion of the VF-1 fluorite sample in the fluid inclusion study; (d) microscopic view of a secondary rooted fluid inclusion of the VF-1 fluorite sample in the fluid inclusion study.

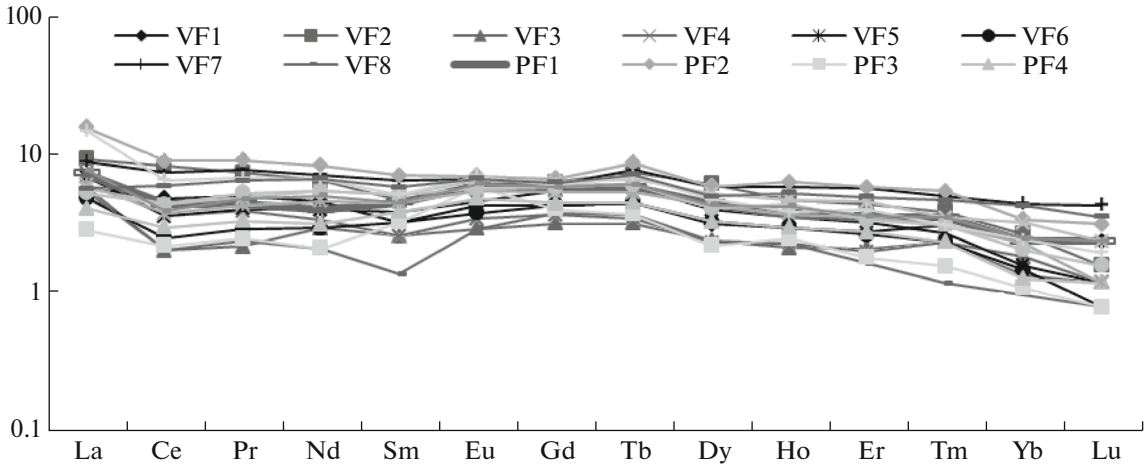


Fig. 12. Rare earth element diagram for the Pohrenk fluorites normalised to the chondrites (Evensen et al., 1978).

A clear fractionation is seen in the normalised REE diagrams of the Pohrenk fluorite samples. There is a slight enrichment in Eu. Compared to other fluorite beds in Central Anatolia (Bayindir, Kaman, Akcakent, Durmuslu etc.), the Pohrenk fluorite beds contain less REE (Uras, 2002). The uniform distribution curve of the Pohrenk fluorite minerals highlights the effect of processes such as alteration and transport. Thus, the light rare earth elements group from La to Eu are the first elements to mix into the solution in a geological time frame. For this reason, it can be assumed that the fluorite crystallised under the influence of solutions depleted in LREE. Moreover, the graph in Fig. 12 shows a slight decrease in light, medium and heavy rare earth elements, becoming near horizontal. The REE content of the fluorites vary between 0.08–5.80 ppm. There is 215.56 ppm REE in a total of 18 fluorite samples (Table 8). The similar Büyükkızılcık and Feke fluorites are relatively poor in rare earth element content (Uras, 2002; Uras and Calıskan, 2014) Also, compared to the other fluorite beds in Central Anatolia (Bayindir, Kaman, Akcakent, Durmuslu

Table 4. Major element content of the Pohrenk fluorites

	SiO_2	Al_2O_3	Fe_2O_3	MgO	CaO	Na_2O	K_2O	TiO_2	P_2O_5	MnO	LOI
VF-1	1.59	0.18	0.08	0.01	95.9	0.01	0.04	0.01	0.04	0.01	1.10
VF-2	0.07	0.03	0.04	0.01	91.3	0.03	0.04	0.01	0.06	0.01	0.50
VF-3	0.08	0.03	0.04	0.01	95.1	0.01	0.04	0.01	0.05	0.01	0.70
VF-4	0.80	0.03	0.04	0.01	96.9	0.02	0.04	0.01	0.02	0.01	0.50
VF-5	0.07	0.03	0.05	0.01	98.1	0.01	0.04	0.01	0.01	0.01	0.30
VF-6	0.15	0.03	0.04	0.02	97.6	0.01	0.04	0.01	0.07	0.01	0.10
VF-7	1.06	0.03	0.04	0.01	97.6	0.02	0.04	0.01	0.03	0.01	0.90
VF-8	0.11	0.03	0.04	0.01	97.8	0.01	0.04	0.01	0.01	0.01	0.10
VF-9	29.61	0.09	0.07	0.01	67.8	0.01	0.04	0.01	0.01	0.01	4.20
PF-1	0.08	0.03	0.04	0.01	98.6	0.03	0.04	0.01	0.03	0.01	0.60
PF-2	0.08	0.03	0.09	0.01	96.8	0.03	0.04	0.01	0.04	0.01	0.60
PF-3	0.11	0.03	0.04	0.01	96.9	0.01	0.04	0.01	0.03	0.01	0.60
PF-4	0.06	0.03	0.04	0.01	97.6	0.02	0.04	0.01	0.03	0.01	0.60
PF-5	0.11	0.03	0.04	0.01	95.4	0.03	0.04	0.01	0.02	0.01	0.30
PF-6	0.07	0.03	0.08	0.05	95.8	0.02	0.04	0.01	0.01	0.01	0.30
PF-7	0.08	0.03	0.05	0.01	97.9	0.03	0.04	0.01	0.06	0.01	0.50
PF-8	0.12	0.03	0.04	0.01	95.6	0.03	0.04	0.01	0.04	0.01	0.60
PF-9	0.08	0.03	0.09	0.01	98.7	0.03	0.04	0.01	0.05	0.01	0.50
PF-10	0.15	0.03	0.10	0.01	95.7	0.03	0.04	0.01	0.01	0.01	0.30

Table 5. Trace element content of the Pohrenk fluorite

	Sc	Ba	Be	Cs	Rb	Sr	Ta	Th	U	V	W	Zr
VF-1	1.00	611.4	1.00	0.10	0.5	39.8	0.1	0.1	0.40	5.00	0.10	0.90
VF-2	1.00	1751.8	1.00	0.1	0.5	71.3	0.10	2.20	0.30	5.00	0.1	0.50
VF-3	1.00	64.3	1.00	0.1	0.5	50.2	0.10	0.1	0.20	5.00	0.1	0.50
VF-4	1.00	60.7	1.00	0.10	0.5	31.0	0.10	0.30	0.10	5.00	0.10	0.50
VF-5	1.00	5.90	1.00	0.1	0.5	40.0	0.10	0.50	0.20	5.00	0.10	0.50
VF-6	1.00	4.50	1.00	0.1	0.5	33.7	0.10	0.10	0.10	5.00	0.10	0.50
VF-7	2.00	460.2	1.00	0.10	0.5	44.4	0.10	0.1	0.80	5.00	0.10	0.50
VF-8	1.00	9.30	1.00	0.10	0.50	38.2	0.1	0.50	0.20	5.00	0.10	0.50
VF-9	1.00	15.0	1.00	0.10	0.50	43.2	0.10	0.10	0.60	9.00	3.40	0.60
PF-1	2.00	407.7	1.00	0.10	0.50	67.7	0.10	0.10	0.80	5.00	1.90	0.50
PF-2	1.00	354.1	1.00	0.10	0.50	60.9	0.10	0.30	0.60	5.00	0.10	0.50
PF-3	1.00	42.4	1.00	0.10	0.50	36.9	0.10	0.40	0.10	5.00	0.10	0.50
PF-4	1.00	206.3	1.00	0.10	0.50	39.2	0.10	0.20	0.20	5.00	0.10	0.50
PF-5	3.00	108.6	1.00	0.10	0.50	55.7	0.10	0.30	0.60	5.00	0.10	0.50
PF-6	2.00	19.6	1.00	0.10	0.50	49.9	0.10	0.70	0.60	5.00	0.90	0.50
PF-7	1.00	87.7	1.00	0.10	0.50	49.6	0.10	0.50	0.30	5.00	0.10	0.50
PF-8	1.00	545.0	1.00	0.10	0.50	62.8	0.10	0.10	0.70	6.00	0.20	0.80
PF-9	2.00	56.1	1.00	0.10	0.50	59.7	0.10	0.10	0.50	5.00	0.10	0.50
PF-10	3.00	6.60	1.00	0.10	0.50	57.9	0.10	0.40	1.00	5.00	0.10	0.60

etc.), the Pohrenk fluorite beds contain less REE (Uras et al., 2002). In this study, the rare earth element content was normalised to C1-Chondrites (Evevsen et al., 1978) (Fig. 12). According to (Constantopoulos, 1988), if the Eu/Eu* values are >1, as there is enough oxygen in the environment Eu^{+2} becomes oxidised to Eu^{+3} and gets incorporated into the fluorite structure. If the Ce/Ce* values are <1, the Ce bonds with oxygen to deposit out of solution as CeO_2 and is therefore prevented from becoming part of the fluorite structure. This situation could be associated with a pluton. The Ce/Ce* and Eu/Eu* ratios have been formalised as $Ce/Ce^* = Ce_n/(La_n \times Pr_n)^{1/2}$ and $Eu/Eu^* = Eu_n/(Sm_n \times Gd_n)^{1/2}$ (Table 8) (Möller et al., 1983, Constantopoulos, 1988, Palmer et all., 1996; Jones et al., 2000). As the Eu anomaly observed in the Pohrenk fluorites is positive, it is simple to go from feldspathic, detrital or magmatic rocks to natural solutions in diagrams normalised with chondritic values (Table 8). In the Eu and Ce anomalies, high temperatures (T) and a high fO_2 environment is indicated by positive Eu and negative Ce anomalies. The occurrence of REE's as a complex structured mineral shared with fluorite can explain this. Like fluorite, it takes REE into its structure; however it shares the lanthanide sources with fluorite to give a positive Eu anomaly. The negativity of the Ce anomaly is an indicator of excess oxygen in the environment (Rollinson, 1993). The Ce/Yb ratios of the Pöhrenk fluorites represent the light rare earth element (LREE) situation. According to this situation, there is a decrease in LREE in Table 8. In the Tb/Ca and Tb/La diagrams by (Schneider et all., 1975) for pegmatitic, hydrothermal and sedimentary fluorites, it is seen that the Pohrenk fluorites are situated in the hydrothermal rooted area (Fig. 13).

The Pohrenk fluorites were formed under the effect of hydrothermal waters. The presence of high value cations of the fluorites (HFS) and rare earth element values being low compared to the wall rocks show that these elements were affected by mineralising fluids (Yaman, 1985). In the $(Tb/Yb)_n - (La/Yb)_n$ diagram by (Hill et al., 2000) the Pohrenk fluorite samples that were studied plot in the Akdagmadeni fluorites (Sasmaz et al., 2005) Buyukkizilcik fluorites (Uras and Calıskan, 2014) and Lordsburg Steeple Rock area (Fig. 14a). It appears from the evidence that there was crystallisation and loss of LREE at an early stage in the Pohrenk fluorites. This reduction can be seen in the LREE and the positive Eu anomalies of the Pohrenk fluorites in the $(La/Yb)_n - (Eu/Eu^*)_n$ diagram (Fig. 14b). The Pohrenk fluorites show similar properties to the Akdagmadeni fluorites (Sasmaz et al., 2005) and Buyukkizilcik fluorites (Uras and Calıskan, 2014) in the Sc/Eu and Sr diagram and plot in a limited area on the diagram when rich in Sr (Fig. 16). Enrichment in Sr content and positive Eu anomalies can be seen in the $Sr - (Eu/Eu^*)_n$ diagram

Table 6. The major element content of the formations, and the clay, barite, nummulite and travertine of the Dulkadir limestone member surrounding the Pohrenk fluorite

	SiO_2	Al_2O_3	Fe_2O_3	MgO	CaO	Na_2O	K_2O	TiO_2	P_2O_5	MnO	Cr_2O_3	LOI
A-2	86.00	5.79	0.62	0.32	1.5	0.04	0.63	0.34	0.06	0.01	0.02	7.00
A-4	71.54	14.87	2.13	0.90	0.6	0.04	1.82	0.69	0.23	0.01	0.01	7.30
A-5	67.43	15.10	3.71	1.18	0.7	0.05	2.33	0.74	0.21	0.01	0.01	8.70
A-6	64.90	22.02	0.88	0.38	0.4	0.03	0.74	0.81	0.12	0.01	0.01	9.80
A-7	51.64	15.30	2.45	0.52	11.8	0.03	1.08	0.65	0.25	0.01	0.01	16.30
A-8	58.38	15.56	4.85	1.07	5.5	0.04	2.07	0.73	0.27	0.01	0.01	11.60
A-9	51.89	12.87	4.02	1.06	11.8	0.03	1.94	0.61	0.15	0.02	0.01	12.20
A-10	63.17	15.92	5.44	1.43	0.8	0.04	2.47	0.78	0.18	0.01	0.01	9.90
A-11	16.05	4.23	1.34	0.35	41.9	0.01	0.48	0.18	0.05	0.01	0.01	35.40
A-14	81.90	9.30	0.77	0.33	1.5	0.06	0.77	0.54	0.19	0.01	0.02	7.00
A-15	70.65	6.78	0.95	0.26	12.2	0.04	0.63	0.40	0.17	0.01	0.01	7.80
KC-5	55.95	5.67	0.94	0.36	20.0	0.08	0.64	0.27	0.07	0.01	0.01	10.10
KJ-1	2.03	0.61	0.20	0.18	50.2	0.01	0.05	0.02	0.03	0.01	0.001	40.50
KO-1	65.56	12.85	4.42	1.94	0.9	0.42	2.91	0.63	0.73	0.01	0.02	9.50
BT-1	0.35	0.07	0.04	0.01	0.2	0.01	0.04	0.01	0.01	0.01	0.001	0.10
NT-1	1.29	0.41	0.12	0.12	55.9	0.01	0.04	0.02	0.02	0.01	0.00	41.90
NK-1	6.17	1.43	0.24	0.18	52.0	0.01	0.08	0.06	0.01	0.02	0.00	39.60
NK-2	67.51	15.82	2.47	0.87	1.8	0.04	1.15	0.67	0.14	0.01	0.06	9.20
TB-1	81.60	9.71	1.38	0.46	0.4	0.04	1.13	0.47	0.12	0.01	0.01	4.80
TB-2	81.45	10.68	0.58	0.41	0.2	0.03	1.05	0.52	0.04	0.01	0.01	5.10
TB-3	85.70	7.87	0.51	0.37	0.2	0.03	0.94	0.40	0.11	0.01	0.01	3.90
TB-4	84.87	7.15	2.46	0.29	0.2	0.03	0.80	0.36	0.11	0.01	0.01	3.80
TB-5	87.72	6.53	0.46	0.32	0.2	0.03	0.86	0.34	0.09	0.01	0.01	3.50
TB-6	85.80	6.92	1.93	0.34	0.2	0.04	0.87	0.35	0.11	0.01	0.01	3.50
TB-8	57.39	7.55	0.54	0.24	15.4	0.11	0.59	0.34	9.24	0.01	0.01	5.80
TB-9	79.22	10.23	1.16	0.31	1.8	0.05	0.76	0.48	0.95	0.01	0.01	5.00
TB-10	83.22	9.55	0.93	0.27	0.1	0.06	0.73	0.46	0.06	0.01	0.01	4.60
TB-11	83.52	9.29	0.38	0.31	0.2	0.02	0.80	0.47	0.10	0.01	0.01	4.90
TB-12	83.84	8.26	1.23	0.37	0.2	0.03	0.89	0.41	0.14	0.01	0.01	4.30
TB-13	83.07	8.73	1.67	0.37	0.2	0.03	0.90	0.42	0.16	0.01	0.01	4.30
TBH-1	1.12	0.38	1.22	0.31	54.2	0.19	0.10	0.01	0.02	0.01	0.001	42.40

(Fig. 17). The Sc content of the Pohrenk fluorite plots in a similar area on the diagram to the Akdagmadeni (Sasmaz et all., 2005) and Buyukkizilcik fluorite (Fig. 18).

7. Sr AND Nd ISOTOPES

Nd–Sr (ID + IC) analysis of the Pohrenk fluorites was completed using 3 pure fluorite (PF-1, PF-2, VF-1) samples. In the analysis results, it is found that the Pohrenk fluorite samples plot in the enriched zone outside the mantle area of the Nd–Sr diagram (Fig. 15). The $^{143}Nd/^{144}Nd$ values of samples vary between 0.512349 and 0.512497 whilst $^{87}Sr/^{86}Sr$ values vary between 0.708161 and 0.708772 (Table 9). The Sm–Nd values of the samples give an isochron age on the age graphic. This situation can be explained by the young age of the samples, the different time gaps and feeding from the source which disrupted the isotopic balance. Although the formation age of the samples cannot be calculated isotopically, from field relationships it is known that they formed post-Eocene. For the samples from the Oligocene and Miocene Epochs for which beginning Nd–Sr isotope values were calculated, it is

Table 7. The trace element content of the formations, and the clay, travertine and nummulite of the Dulkadir limestone member surrounding the Pohrenk fluorite

	Sc	Ba	Be	Co	Cs	Ga	Hf	Nb	Rb	Sr	Ta	Th	U	V	W	Zr
A-2	5	8870	1	1.3	6.20	12.80	1.70	5.00	31.30	238.6	0.40	3.00	3.40	117.00	16.60	62.00
A-4	19	95.2	3	3.9	15.50	16.40	3.20	9.60	75.40	133.9	0.60	11.70	1.70	160.00	6.60	118.50
A-5	17	102	3	11.2	18.30	18.80	3.30	10.50	98.90	145.8	0.60	10.30	1.60	171.00	8.10	130.90
A-6	9	300.1	2	2.6	6.30	20.20	4.00	9.40	28.80	85.5	0.50	7.80	1.40	87.00	20.50	146.30
A-7	15	87.5	1	3.8	7.70	14.20	3.00	7.90	42.70	96.00	0.50	6.80	1.00	131.00	6.70	104.10
A-8	15	165	3	6.6	15.80	16.30	3.30	10.00	81.70	98.7	0.60	80.80	1.50	171.00	5.50	122.70
A-9	12	151	3	8.8	13.80	15.50	2.90	7.90	73.30	105.2	0.60	6.40	1.30	166.00	6.60	100.00
A-10	17	207	5	41.1	15.50	22.40	3.50	10.60	94.80	106.6	0.70	9.00	5.00	286.00	5.30	140.40
A-11	7	64	1	2.2	4.01	4.50	0.80	2.30	18.00	107.6	0.30	1.50	0.50	47.00	0.60	28.00
A-14	6	96.5	1	1.2	6.90	20.60	4.40	7.50	35.30	79.4	0.50	4.10	2.70	145.00	13.30	84.90
A-15	5	1655.3	1	1.6	6.40	18.20	1.60	5.60	28.30	108.9	0.30	2.90	2.20	155.00	11.40	66.70
KC-5	5	46305.4	4	3.4	30.30	21.50	1.80	4.00	56.80	865.9	0.70	3.40	2.50	208.00	37.20	66.10
KJ-1	2	137	1	0.5	0.70	0.60	0.90	0.70	5.30	129.4	0.10	1.90	0.60	5.00	0.30	28.90
KO-1	12	209.4	7	15.6	121.30	36.50	4.40	12.60	290.90	115.8	0.70	10.10	3.10	172.00	50.60	164.00
BT-1	1	330000	1	0.9	0.10	0.5	1.40	0.5	0.50	6737.1	2.70	0.10	0.10	0.5	0.20	1.00
NT-1	3	110	1	1.7	0.40	0.60	0.5	0.5	1.20	106.1	1	2.70	1.30	29.00	0.60	3.40
NK-1	4	575	1	6.4	1.10	1.50	0.5	1.10	3.70	174.1	0.10	2.80	1.80	145.00	1.40	10.30
NK-2	12	616.2	3	10.6	32.60	28.10	3.30	11.70	81.70	115.6	0.70	15.40	9.00	676.00	27.30	109.80
TB-1	8	62.7	3	3.20	6.30	13.40	2.20	6.40	49.20	266.1	0.40	4.90	3.00	106.00	39.10	81.80
TB-2	7	66.3	1	1.50	5.50	12.80	1.90	6.50	43.30	225.50	0.40	4.30	3.40	93.00	4.80	83.50
TB-3	5	254.3	1	0.80	3.80	10.70	1.80	5.30	36.90	555.0	0.30	3.80	2.30	78.00	2.80	67.90
TB-4	5	158.5	1	1.10	3.20	9.20	1.40	4.40	29.00	490.2	0.30	3.30	1.90	110.00	3.20	58.70
TB-5	5	220.5	1	4.20	4.00	9.20	1.70	4.70	34.70	367.3	0.30	3.60	2.20	63.00	52.10	59.10
TB-6	5	252	1	6.20	3.60	9.80	1.50	4.90	33.10	347.8	0.30	2.40	2.10	118.00	83.40	59.00
TB-8	17	22340.2	2	1.90	16.30	12.50	2.30	6.10	39.80	645.9	0.50	4.90	30.70	45.00	10.10	83.90
TB-9	8	679.4	3	1.60	22.70	15.40	3.50	8.30	53.90	76.1	0.60	7.70	6.30	79.00	19.90	119.20
TB-10	5	75.6	3	0.60	3.70	9.70	2.20	5.50	27.90	152.7	0.30	4.50	2.30	81.00	5.80	79.60
TB-11	5	202.9	2	0.90	3.70	10.70	2.00	6.80	32.50	320.6	0.40	4.60	2.40	82.00	4.00	83.60
TB-12	7	1273.2	1	1.90	3.60	7.80	1.80	4.60	33.10	675.3	0.30	3.80	3.20	82.00	12.80	64.10
TB-13	7	999.1	2	2.00	4.20	9.40	2.10	5.00	34.00	764.4	0.30	4.00	2.90	82.00	14.90	65.20
TBH-1	1	102.5	3	0.50	1.40	1.60	0.5	0.5	3.30	273.4	0.1	0.20	0.10	9.00	26.30	4.00

observed that they have low starting $^{143}Nd/^{144}Nd$ values and high starting $^{87}Sr/^{86}Sr$ values. The $\varepsilon Nd_{(t)}$ values of the samples vary between 2.8 and 5.7. Although these values show that the fluorites fed from continental crust, the Rb content and low LREE values of the samples are an indicator of a mantle origin where continental contamination occurred (Table 10). When compared to the Nd–Sr values of magmatics and young volcanics in the region, the Pohrenk fluorites have similar isotopic signatures to the Upper Cretaceous aged magmatics, Early-Middle Miocene volcanics and Mio-Quaternary volcanics. In light of field and geochemical values, it is thought that the fluorite samples can be correlated with Early-Middle Miocene volcanics.

8. RESULTS AND DISCUSSION

The study area is composed of the Pohrenk fluorites that have emplaced into the Dulkadir limestone member. Almost all of the thin sections acquired from the fluorite and wall rocks prepared from the units of the Dulkadir limestone exhibit clay alteration. In these thin sections, the clays form a laminated structure and the marks left by hot water are seen clearly. For this reason, the wavy extinction shown by quartz crystals is thought to be caused by hot water or that the quartz minerals have been affected by pressure and undergone deformation. The carbonate layers were made more apparent by crystallising after enclosing the fluorite, quartz and silicified marl fragments. The fluo-

Table 8. REE content of the Pöhrenk fluorites (Chondrites (Cl) taken from (Evensen et al., 1978)

	La	Ce	Pr	Nd	Sm	Eu	Gd	Tb	Dy	Ho	Er	Tm	Yb	Lu	Ce/Yb	Tb/La	Ca	Tb/Ca × 10^{-8}	Ce/Ce*	Eu/Eu*	TopREE
VF-1	1.40	3.10	0.49	2.20	0.50	0.25	0.88	0.17	0.80	0.17	0.46	0.08	0.39	0.06	38.75	0.121	68.3	0.0117130307	0.90	1.15	10.89
VF-2	2.30	5.30	0.72	3.10	0.90	0.35	1.30	0.28	1.57	0.27	0.74	0.10	0.44	0.04	53.00	0.122	65.2	0.0240797546	0.99	1.01	17.37
VF-3	0.5	1.30	0.21	1.40	0.40	0.17	0.65	0.12	0.61	0.12	0.35	0.06	0.30	0.03	21.67	0.267	67.9	0.0089837997	0.56	1.02	6.14
VF-4	1.80	2.30	0.38	1.60	0.40	0.20	0.75	0.13	0.59	0.13	0.33	0.06	0.22	0.03	38.33	0.072	69.2	0.0085260116	0.66	1.12	8.89
VF-5	1.70	2.30	0.39	1.90	0.60	0.27	1.13	0.22	1.02	0.20	0.54	0.07	0.26	0.03	32.86	0.129	70.1	0.0145506419	0.67	1.07	10.60
VF-6	1.20	1.60	0.28	1.40	0.50	0.22	0.89	0.17	0.84	0.17	0.44	0.06	0.24	0.02	26.67	0.142	69.7	0.0120516499	0.66	1.02	8.01
VF-7	2.20	5.80	0.76	3.40	1.00	0.39	1.25	0.29	1.50	0.33	0.95	0.13	0.73	0.11	44.62	0.132	69.7	0.0215208034	0.89	1.11	18.93
VF-8	0.5	1.30	0.23	1.00	0.40	0.17	0.77	0.14	0.61	0.13	0.27	0.05	0.16	0.02	3.61	0.400	68.9	0.0088534107	0.56	1.04	5.89
PF-1	1.80	2.80	0.43	1.90	0.70	0.35	1.18	0.22	1.13	0.21	0.59	0.09	0.39	0.06	31.11	0.122	70.4	0.0160511364	0.76	1.18	11.79
PF-2	3.90	5.80	0.88	4.00	1.10	0.41	1.38	0.33	1.51	0.36	0.97	0.14	0.56	0.08	41.43	0.085	69.1	0.0218523875	0.75	1.05	21.62
PF-3	0.70	1.40	0.24	1.00	0.50	0.21	0.83	0.14	0.56	0.14	0.30	0.05	0.18	0.02	5.60	0.200	69.2	0.0080924855	0.82	1.06	6.45
PF-4	1.00	1.90	0.32	1.50	0.60	0.24	0.92	0.17	0.84	0.17	0.46	0.06	0.21	0.03	31.67	0.170	69.7	0.0120516499	0.80	1.01	8.39
PF-5	1.40	2.80	0.47	2.60	0.80	0.38	1.31	0.25	1.33	0.27	0.76	0.09	0.53	0.06	31.11	0.179	68.1	0.0195301028	0.83	1.13	12.99
PF-6	1.50	2.40	0.42	2.20	0.70	0.32	1.11	0.20	1.10	0.21	0.59	0.08	0.38	0.03	30.00	0.133	68.4	0.0160818713	0.72	1.11	11.21
PF-7	1.30	2.80	0.51	2.60	0.80	0.33	1.19	0.23	1.05	0.25	0.56	0.08	0.34	0.04	35.00	0.177	69.9	0.0150214592	0.82	1.03	12.04
PF-8	3.70	4.20	0.66	3.20	0.80	0.41	1.24	0.26	1.22	0.22	0.67	0.08	0.40	0.05	52.50	0.070	68.3	0.0178623719	0.64	1.26	17.06
PF-9	1.90	2.50	0.46	2.40	0.70	0.36	1.20	0.23	1.10	0.24	0.60	0.09	0.41	0.06	27.78	0.121	70.5	0.0156028369	0.64	1.20	12.19
PF-10	1.40	3.80	0.63	3.20	0.90	0.39	1.29	0.27	1.27	0.30	0.82	0.12	0.71	0.09	31.67	0.193	68.4	0.0185672515	0.97	1.11	15.10
Cl	**0.245**	**0.638**	**0.096**	**0.474**	**0.154**	**0.058**	**0.204**	**0.037**	**0.254**	**0.057**	**0.166**	**0.026**	**0.165**	**0.025**							215.56

rite enrichment of $CaCO_3$ shells belonging to the nummulites in the nummulite limestone layers was determined both with macro and micro observations. In the typical FTIR and XRD diagrams of all samples, the most dominant minerals are kaolinite and quartz. Apart from kaolin, in some samples smectite-illite and dickite minerals are also seen. According to FTIR analyses, the travertines and wall rock samples are composed of kaolinite, quartz, smectite, apatite and dickite minerals. The values gained from XRD analyses match with the FTIR results. The results of the fluid inclusion studies show that the Pohrenk fluorites formed in a hot (Th: 78.1–363°C) and saline (1.05–24.08% NaCl equivalent) environment. When the major element content of the fluorite samples are studied it is found that, apart from two samples (VF-1 and VF-9), all samples are composed of pure fluorite. Sample VF-9 in particular, is formed of silica and fluorite and its silica phase (Opal $SiO_2 \cdot nH_2O$) contains a considerable amount of water (LOI: 4.2%). Trace element contents of the fluorite samples show important changes. Other samples contain more major and trace elements compared to the fluorites. The HFS (High Field Strength) element content of the fluorites is low when compared to the other samples. This shows that these elements were not affected by the fluids that resulted in the formation of fluorite, and remained stable. Whilst the REE (0.08–5.80 ppm) content of the Pohrenk fluorite beds showed minimal enrichment, the wall rocks alongside the fluorite beds (0.08–34.0 ppm), the wall rocks around the hot water (0.02–234.0 ppm) and the silicified and non-silicified nummulites (0.07–56.0 ppm) showed a greater degree of enrichment compared to the Pohrenk fluorites. In studying the normalised lanthanide diagrams, it is noted that the Pohrenk fluorites and other samples show a decrease in light, medium and heavy rare earth elements, followed by a near horizontal slope. A hydrothermal origin is suggested when the Tb/La and Tb/Ca ratio diagrams of the REE content of the Pohrenk fluorite is investigated. Furthermore, the study by (Koc et al., 2001) showed that the Pohrenk fluorite had a hydrothermal origin. The Büyükkızılcık fluorites crystallised at an early stage (Möller et all., 1976; Möller et al., 1983). The fluorite studied is honey-yellow. The negative Ce and positive Eu anomalies observed in the Pohrenk fluorites indicates high (T) and fO_2 at the source hydrothermal fluids (Constantopoulos, 1988; Palmer et al., 1996; Hill and Kyle, 2000). All values along the NS trending Pohrenk faults

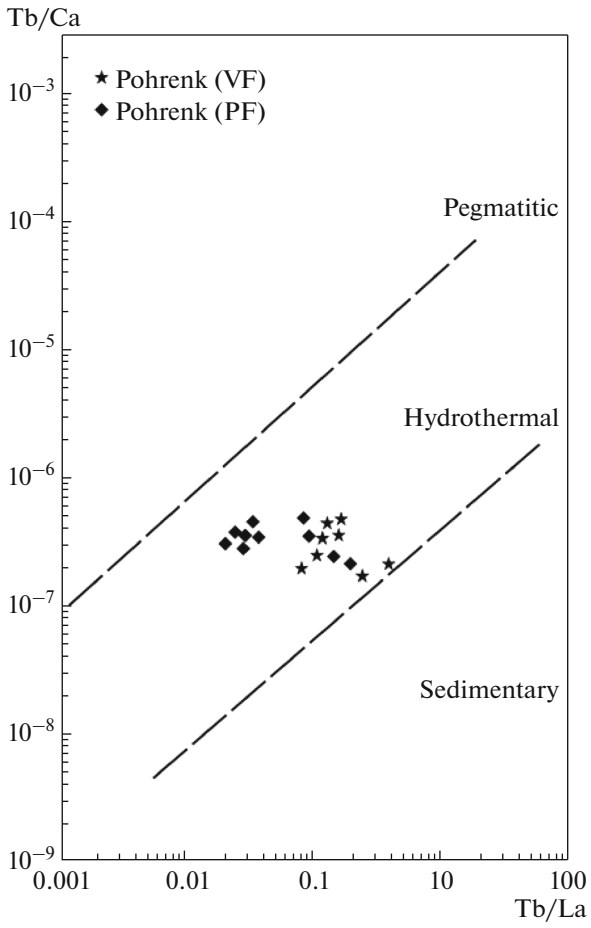


Fig. 13. Plot of Tb/Ca versus Tb/La in fluorites from the Pohrenk area.

show that geothermal activity reaches the surface. For this reason, it can be said that the faults play a major role in the silicification and fluorite activity. The fact that the NS trending faults are covered by Pliocene aged units shows that the faults became active before the Pliocene. This activity likely relates to the Central Anatolian Upper Miocene volcanics. These findings match well with the post-Paleocene ages proposed for the fluorite veins seen in the Central Anatolian crystalline massifs.

The total REE content and high Sc values of the Pohrenk fluorites are seen in the total Sc-REE diagram. They plot in a similar place on the diagram as

Table 9. Sr and Rb isotope data for the representative Pohrenk fluorite samples

	[Rb] ppm	[Sr] ppm	$^{87}Rb/^{86}Sr$	$^{87}Sr/^{86}Sr$	Err 2s(abs)
PF-1	0.0000	16.2	0.0000	0.708772	0.000010
PF-2	0.0000	29.5	0.0000	0.708161	0.000012
VF-1	0.0000	28.7	0.0000	0.708350	0.000011

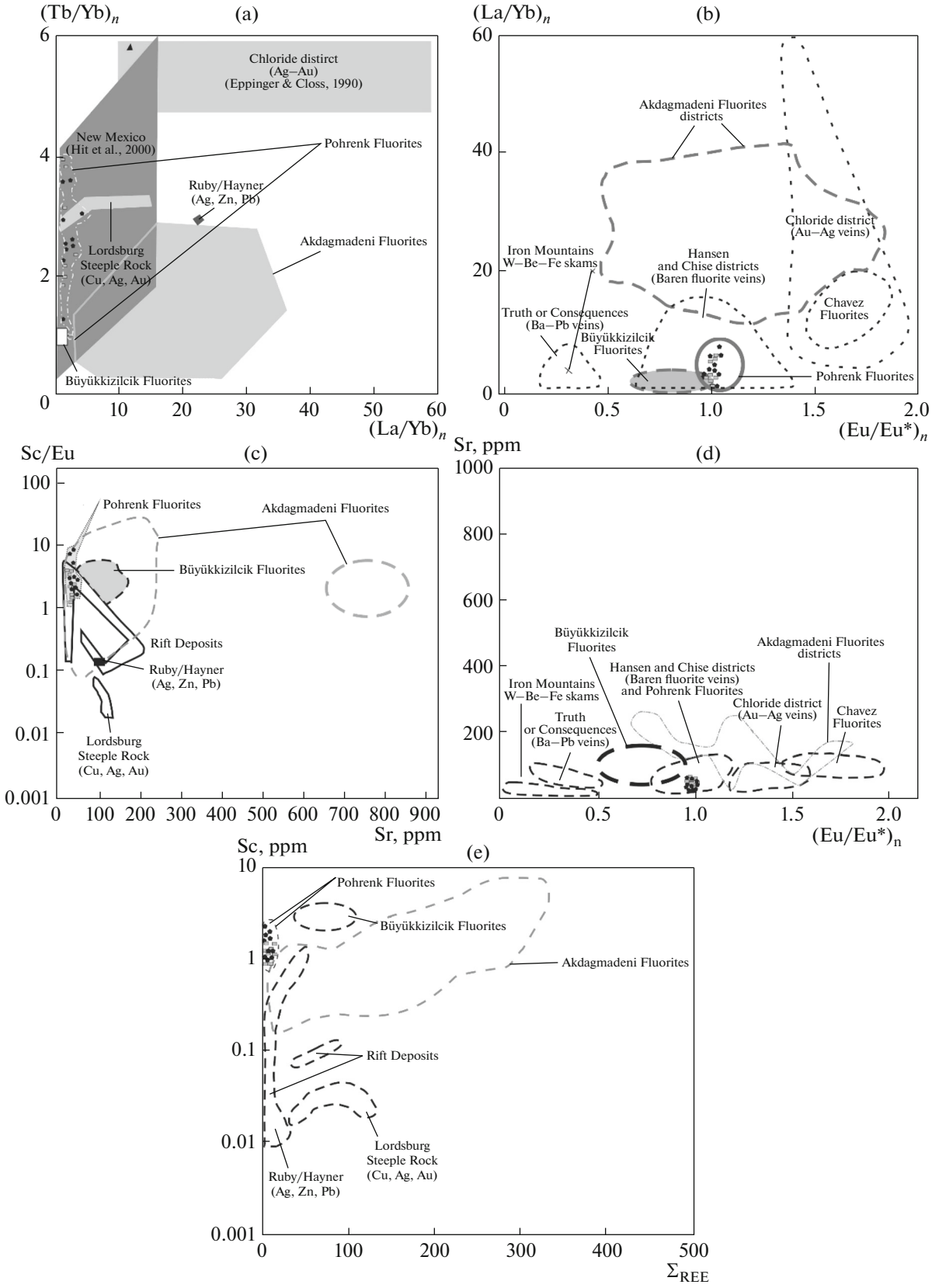


Fig. 14. (a) $(Tb/Yb)_n$ ratio versus $(La/Yb)_n$ ratio of the studied Pöhrenk fluorites. All values are normalized to chondritic meteorites. Büyükkızılcık fluorites are characterized by low Tb/Yb ratios. (b) Chondrite normalized to $(La/Yb)_n$ versus $(Eu/Eu^*)_n$ diagram showing the distribution of samples; (c) Sc/Eu ratios versus Sr content; (d) Sr versus $(Eu/Eu^*)_n$ diagram; (e) Sc versus the sum of analysed REE.

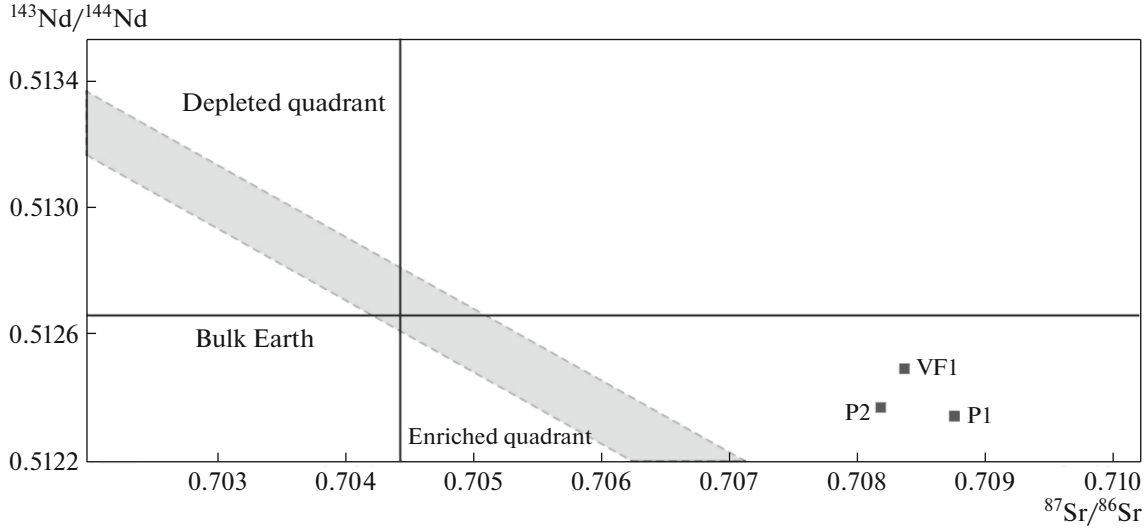


Fig. 15. $^{143}Nd/^{144}Nd$ and $^{87}Sr/^{86}Sr$ diagram.

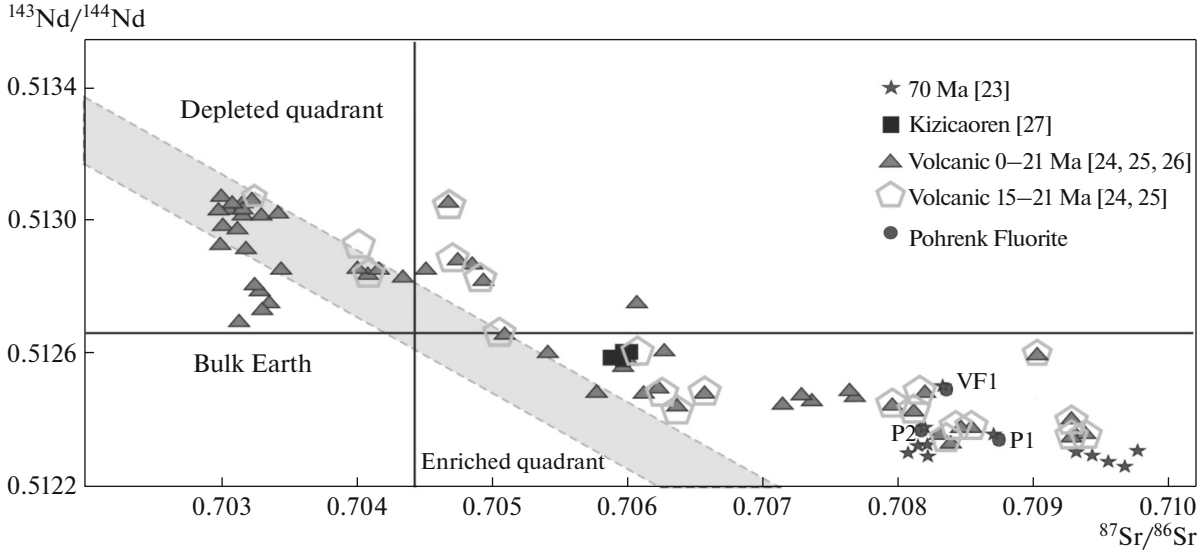


Fig. 16. $^{143}Nd/^{144}Nd$ and $^{87}Sr/^{86}Sr$ diagram (Ilbeyli et al., 2004; Aldanmaz, 1998; Chakrabarti et al., 2011; Dilek and Altunkaynak, 2010; Nikiforova et al., 2014).

the Akdağmadeni fluorites (Sasmaz and Büyükkızılcık fluorites (Fig. 10).

The Pohrenk fluorites contain low values of Sr. In fluorite this value is 67.7 ppm Sr. This is a result of mineral formation from a low degree fractionation. The Pohrenk fluorites show a similar ratio to the Akçadağmadeni and Büyükkızılcık fluorites [19] of the Yozgat region (Fig. 14d). In the Sr – $(Eu/Eu^*)_n$ diagram, similar to the Büyükkızılcık fluorites, the Pohrenk fluorites show low $(Tb/Yb)_n$ and $(La/Yb)_n$ ratios (Figs. 14a, 14b). Some of the Sr – $(Eu/Eu^*)_n$ ratios of the Pohrenk fluorites plot on the Hansen and

Table 10. Sr and Nd isotope data for the representative Pohrenk fluorite samples

	[Sm] ppm	[Nd] ppm	$^{147}Sm/^{144}Nd$	err(abs)	$^{143}Nd/^{144}Nd$	err(abs)
PF-1	0.25	0.65	0.23351	0.00004	0.512349	0.000010
PF-2	0.43	1.35	0.19228	0.00003	0.512370	0.000010
VF-1	0.47	1.32	0.21403	0.00003	0.512497	0.000010

Chise District boundary in the Rio Grande Rift area (Figs. 14a, 14b, 14c, 14d, 14e). The Pohrenk fluorites were plotted on graphs from (Eppinger, 1988; Eppinger and Closs, 1990; Sasmaz et al., 2005) and with data from other fluorite beds.

Nd–Sr analyses completed by other researchers in previous studies conducted in Western Anatolia were considered along with the Pohrenk fluorites. It is observed that the Nd–Sr isotope results of this study plot in the same place on the graph as results of the (Ilbeyli et al., 2004) study (Fig. 16). This shows us that they have similar isotopic signatures. Nd–Sr isotope analyses from other researchers plot around Nd–Sr isotope analyses of the Pohrenk fluorites (Aldanmaz, 1998; Chakrabarti et al., 2011; Dilek and Altunkaynak, 2010; Nikiforova et al., 2014).

9. CONCLUSIONS

The formation model for the Pohrenk fluorites affected by the hot waters in the area was put together following a study into the REE geochemistry, petrography and fluorite isotopes of the fluorites and wall rocks in the Pohrenk Bezirgan area situated in Kırşehir. The 1/25000 scale geology map of the study area was re-prepared as a revised edition of the MTA 1991 version. Geology and paragenesis observations show that the mineralisation developed in the Eocene aged silicified marl and limestone layers. Silicification and fluorite mineralisation is controlled by the NS trending fault. The Pohrenk fluorites have a very low REE content and formed in a scattered manner in an area made of limestone (Bezirgan area). The formation of this formation could have been simplified by positive tectonic failure. The positive Eu anomaly shows high T and high fO_2. The normalised contents and REE diagrams of the Pohrenk fluorites show a hydrothermal source. In light of the fluid inclusion results, after forming the first fluorite crystals at high temperatures, the hydrothermal solution becomes increasingly diluted in salt and likely mixes with meteoric waters. As a result, it is thought that the Pohrenk fluorite crystals started forming in a hydrothermal-mesothermal phase, and continued into the epithermal phase. When compared to Nd–Sr values of magmatics and young volcanics in the region, the Pohrenk fluorites show similar isotopic signatures to Upper Cretaceous aged magmatics, Early-Middle Miocene volcanics and Mio-Quaternary volcanics. Field values and geochemical values show that the fluorite samples could be correlated with Early-Middle Miocene volcanics.

ACKNOWLEDGMENTS

This study was funded and supported by a Scientific Research Support Fund from the Kahramanmaras Sutcu Imam University. This paper is dedicated to the memory of late Prof. Dr. Servet Yaman, who supported me during my studies on fluorites.

REFERENCES

E. Aldanmaz, "Petrogenesis of late cenozoic collision volcanism in western Anatolia, Turkey", Durham theses, (Durham University, 1998). http://etheses.dur.ac.uk/4658/

R. J. Bodnar "Revised equation and table for determining the freezing point depression of H_2O–NaCl solutions" Geochim. Cosmochim Acta **57,** 683–684 (1993).

R. Chakrabarti, A. R. Basu, A. Ghatak, "Chemical geodynamics of Western Anatolian" Int. Geol. Rev., iFirst article, 1–22 (2011).

V. Chernyshev, N. I. Serdyuk, D. Z. Zhuravlev, et al., "High-Precision Strontium Isotopic Analysis Using One-Filament Ionization Mode," in *Mass Spectrometry and Isotopic Geology* (Nauka, Moscow, 1983), pp. 30–43 [in Russian].

J. Constantopoulos, "Fluid inclusion and REE geochemistry of fluorite from south–central Idaho," Econ. Geol. **83**, 626–636 (1988).

Y. Dilek, S. Altunkaynak, "Geochemistry of Neogene–Quaternary alkaline volcanism in western Anatolia, Turkey, and implications for the Aegean mantle" Int. Geol. Rev. **52** (4–6), 631–655 (2010).

R. G. Eppinger, "Trace and REE variation in fluorites collected from skarn and epithermal mineral deposits in the Sierra Cuchillo area, southcentral New Mexico," U.S. Geol. Surv., Open_File Rept. 88_0566 (1988).

G. E. Eppinger and L. G. Closs, "Variation of trace elements and rare earth elements in fluorite: a possible tool for exploration," Econ. Geol. **85**, 1896–1907 (1990).

N. M. Evensen, P. J. Hamilton, and R. K. O'Nions,"Rare earth abundances in chondritic meteorite," Geochim. Cosmochim. Acta **42**, 1199–1212 (1978).

G. T. Hill, A. R. Campbell, and P. R. Kyle, "Geochemistry of southwestern New Mexico fluorite occurrences:implications for precious metals exploration in fluorite bearing systems," J. Geochem. Explor. **8**, 1–20 (2000).

N. İlbeyli, J.A. Pearce, M. F. Thirlwall, and J. G. Mitchell, "Petrogenesis Of Collision-Related Plutonics In Central Anatolia, Turkey", Lithos **72**, 163–182 (2004),

S. Koc and A. Recber, "Fluid inclusion studies and geochemistry of rare earth elements (REE) of hydrothermal fluorites from Pöhrenk (Kırşehir, Central, Turkey)," Acta Geol. Sinica Geol. Soc. China **75** (1), 59–65 (2001).

P. Möller and G. Morteani, "On the chemical fractionation of REE during the formation of Ca minerals and its application to problems of the genesis of ore deposits," in *The Significance of Trace Elements innSolving Petro_-Genetic Problems,* Ed. by S. Augustithis (Athens, 1983), pp. 747–791.

P. Möller, P. P. Parekh, and H. J. Schneider, "The application of Tb/Ca–Tb/La abundance ratios to problems of flourspar genesis," Miner. Deposita **11**, 111–116 (1976).

MTA. (General Directorate of Mineral Research and Exploration) Türkiye Jeoloji Haritası 1 : 100000 ölçekli Kırşehir G 18 Paftası Maden Tetkik ve Arama Genel Müdürlüğü Sf 1–12 (1991)

A. V. Nikiforova, H. Öztürkb, S. Altuncuc, and V. A. Lebedeva, "Kizilcaören orebearing complex with carbonatites (Northwestern Anatolia, Turkey): formation time and mineralogy of rocks" Geol. Ore Deposits, **56** (1), 35–60 (2014).

F. Y Oktay, Savcılı (KAMAN) Cevresinde Orta Anadolu Masifi Tortul Örtüsünün Jeolojisi ve Sedimentolojisi (İ.T.Ü Maden Fakültesi, Docentlik Tezi, İstanbul 1981).

D. A. S. Palmer and A. E. Williams-Jones, "Genesis of the carbonatite-hosted fluorite deposit at Amba Dongar, India: Evidence from fluid inclusions, stable isotopes and whole rock_mineral geochemistry," Econ. Geol. **91**, 934–950 (1996).

H. Rollinson, Using Geochemical Data: Evaluation, Presentation, Interpretation (Harlow, Longman, 1993).

A. Sasmaz, F. Yavuz, A. Sagıroglu, and B. Akgül, "Geochemical patterns of the Akda madeni (Yozgat, Central Turkey) fluorite deposits and implications," J. Asian Earth Sci. **24**, 469–479 2005).

H.-J. Schneider, P. Möller, and P. P. Parekh, "Rare earth elements distribution in fluorites and carbonate sediments of the East-Alpine mid-Triassic sequences in the Nordliche Kalkalpen," Miner. Deposita **10**, 330– 344 (1975).

Y. Uras and C. B. Ersu, F. Oner, "Environmental implications of a hydrogeochemical survey for drinking water in Kirsehir region" Geochem. Int. **49** (11), 1145–1153 (2011).

Y. Uras, *Feke (Adana) ve Baytndtr (Kaman) Fluoritlerinin Nadir Toprak Elementlerinin Karstlatırtlması* (Çukurova University, 2002).

Y. Uras and V. Caliskan, "Geochemical patterns of the Buyukkizilcik (Kahramanmaras) fluorite deposits," Geochem. Int. **52** (12), 1087–1100 (2014)

S. Yaman, "Baytndtr (Kaman) Florid filonlartnda nadir toprak elementleri," Jeokimyast, (Jeoloji mühendisligi **25**, 39–44 (1985).

A. E. Williams-Jones, I. M. Samson, and G.R. Olivo, "The genesis of hydrothermal fluorite_REE deposits in the Gallinas Mountains, New Mexico," Econ. Geol. **95**, 327–342 (2000).

D. Z. Zhuravlev, I. V. Chernyshov, A. A. Agapova, and N. I. Serdyuk, "High-precision neodymium isotopic analysis of rocks," Izv. Akad. Nauk SSSR, Ser. Geol., No. 12, 23–40 (1983).